Available online at www.sciencedirect.com
ScienceDirect
International Journal of Heat and Mass Transfer 51 (2008) 3869–3881
International Journal of HEAT and MASS TRANSFER
www.elsevier.com/locate/ijhmt

A dual reciprocity boundary element method for photothermal interactions in laser-induced thermotherapy

Jianhua Zhou, Yuwen Zhang *, J.K. Chen

Department of Mechanical and Aerospace Engineering, University of Missouri, Columbia, MO 65211, USA

Received 13 August 2007; received in revised form 10 January 2008
Available online 3 March 2008

Abstract

Laser-induced thermotherapy (LITT) is a minimally invasive laser hyperthermia procedure for the treatment of localized tumors. Mathematical modeling of the photothermal processes in laser-irradiated tissues is essential for optimal treatment planning. In this study, A Monte Carlo method is introduced to simulate photon transport in the tumor tissues with complex geometries. The dual reciprocity boundary element method (DRBEM) is then formulated to solve the bioheat transfer equation in the tumors. The model is validated with the finite difference solutions. To illustrate the applications of the proposed DRBEM, several laser delivery schemes, including external laser irradiation, single or multiple laser fiber delivery applicators, are studied for tumors with regular or irregular geometric shapes. The temperature transients, laser energy distribution and coagulation patterns for different laser delivery modes are demonstrated. The unique advantages of the DRBEM, such as easy adaptability to complex tumor geometries and no need to discretize the inner domain, may make it well-suited and robust approach for predicting and controlling the temperature evolution in laser-induced thermotherapy procedure.

Keywords: Dual reciprocity BEM; Monte Carlo simulation; Bioheat transfer; Laser-induced thermotherapy

1. Introduction

Laser-induced thermotherapy (LITT) has been investigated and used clinically for more than two decades as a minimally invasive method for treating different types of tumors in the liver, brain, head and neck, etc. [1]. In the LITT procedure, a near-infrared laser radiation is delivered to the targeted area via an external laser beam irradiated on the skin surface or by inserting a scattering laser fiber applicator into the tumor center (the latter is referred to as *interstitial laser thermotherapy*, ILT). The targeted pathological tissue is destroyed by the immediate or delayed hyperthermic and coagulative effects due to photon absorption and heat transfer in the tissue [2,3].

Ideally, the goal of LITT is to enable total pathological cell death and to minimize damage to surrounding healthy tissue, especially in vital organs. Therefore, mathematical models and/or real-time monitoring experimental techniques are indispensable for planning, control and verification of the treatment effect. Most of the real-time monitoring experimental techniques are subject to some drawbacks such as patient discomfort, poor resolution, radiation exposure, etc. [4,5].

On the other hand, theoretical modeling of the laser-tissue interaction process is an important and effective means to facilitate the evaluation of a wide range of parameters (e.g., laser wavelength, laser duration time, and total delivered energy) for a desired outcome. Although many theoretical studies have been conducted to investigate the hyperthermic and coagulative responses of tissue during LITT (e.g., [6–14]), most of the previous models were proposed for biological tissues with regular geometries. In reality, the tumors can have different sizes and shapes

* Corresponding author. Tel.: +1 573 884 6936; fax: +1 573 884 5090.
E-mail address: zhangyu@missouri.edu (Y. Zhang).

0017-9310/$ - see front matter © 2008 Elsevier Ltd. All rights reserved.
doi:10.1016/j.ijheatmasstransfer.2008.01.009

Nomenclature

c_b	specific heat of blood, J/kg K
c_p	specific heat of tissue, J/kg K
f_j	expansion functions
k	thermal conductivity of tissue, W/m K
l_c	characteristic length, m
L	number of BEM internal nodes
$L(\bar{r},\hat{s})$	laser intensity, W/m^2 sr
L_x, L_y, L_z	the lengths in x, y and z directions, m
N	number of BEM boundary nodes
N_p	total photon number in Monte Carlo simulation
n	refractive index
$p(\hat{s},\hat{s}')$	phase function for single scattering
P	laser power, W
q_l	heat generation due to laser absorption in tissue, W/m^3
Q_l	non-dimensional heat generation due to laser absorption
q_m	metabolic heat generation, W/m^3
Q_m	non-dimensional metabolic heat generation
r_j	the radial distance from the DR collocation point j, m
$\bar{r}$	position vector in radiative transfer equation, m
s	stepsize of photon movement, m
$\hat{s},\hat{s}'$	direction vectors
t	time, s
T	tissue temperature, °C
T_a	temperature of the supplying arterial blood, °C
T_c	characteristic temperature, °C
u	non-dimensional temperature
u_a	non-dimensional arterial blood temperature
u^*	fundamental solution of Poisson equation
w_b	blood perfusion rate, m^3/m^3 tissue s
W	photon weight
x, y, z	coordinate variables, m
X, Y, Z	non-dimensional coordinate variables

Greek symbols

α	thermal diffusivity of tissue, m^2/s
ϕ	azimuthal angle in photon scattering, rad
μ_t	attenuation coefficient, m^{-1}
μ_a	absorption coefficient, m^{-1}
μ_s	scattering coefficient, m^{-1}
μ_x, μ_y, μ_z	direction cosines for photon movement
θ	deflection angle in photon scattering, rad
ρ	density of tissue, kg/m^3
ρ_b	density of blood, kg/m^3
ω'	solid angle, sr
ξ, ξ_1, ξ_2, ξ_3	random numbers in the interval (0, 1)

depending on the different organs and disease stages [15]. To establish a theoretical model that has a good adaptability to complex tumor shapes, we must resort to new numerical algorithms to predict the photothermal processes occurring in laser-induced thermotherapy. Among the existing numerical methods, the finite difference method (FDM) is not convenient for the establishing of such a model due to its poor adaptability to complex geometries. Therefore, some researchers attempted to use the finite element method (FEM) to predict the transient temperature distribution in laser-irradiated biological tissues (e.g. [16–18]). But the FEM involves large computational costs (memory and CPU time) since it is a domain-based numerical technique that requires discretizing the space everywhere inside the entire computational domain.

In recent years, the boundary element method (BEM) has been stimulating more and more interests as a powerful tool for analyzing heat transfer processes in biological systems since its first application in bioheat transfer area [19]. Compared with the FDM and FEM methods, BEM has unique ability to provide a complete problem solution in terms of boundary values only, with substantial savings in computer time and data preparation [20–22]. However, there exist two severe restrictions in the traditional BEM for solving the bioheat transfer equation (BHTE) in laser-irradiated tissues. The first is that the fundamental solution to the BHTE with the non-homogeneous blood perfusion term is very difficult to obtain, thus the equivalent boundary integral equation is not available. The sec-

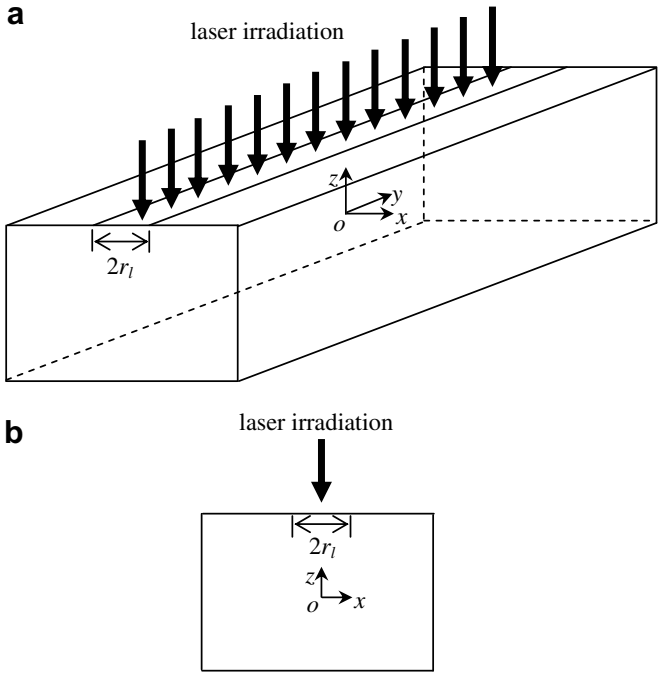

Fig. 1. The Cartesian coordinate systems used in the Monte Carlo simulation.

ond restriction is that the volumetric heat generation term arising from laser light absorption needs to be included in the BEM formulation by means of domain integrals, which detracts from the boundary-only feature of the BEM technique. Fortunately, the above-mentioned difficulties can be overcome using the dual reciprocity boundary element method (DRBEM). Since its first introduction by Nardini and Brebbia [23], the DRBEM has been successfully applied to various thermophysical problems [24] including bioheat transfer problems [25,26]. However, it has not been reported to simulate the photothermal responses of biological tissues in laser-induced thermotherapy, which needs to consider the photon propagation in turbid tissues with complex geometries as well as the effects of blood perfusion and metabolic heat generation.

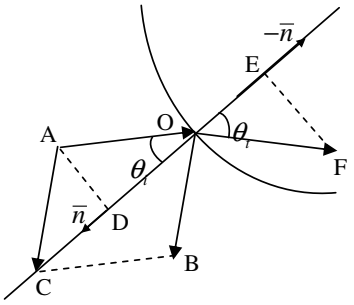

Fig. 2. The geometry used for describing the reflection and transmittance behavior at a boundary with arbitrary geometry.

In this study, a DRBEM model is developed to solve the photothermal interactions in laser induced thermotherapy. The transient temperature elevation is predicted by the bioheat equation taking into account the blood perfusion term. The Monte Carlo approach is applied to simulate the photon transport in laser irradiated tissues. Three different tumor shapes, i.e., square, circle and ellipse, and various laser delivery modes, i.e., external laser irradiation, single and multiple laser fiber schemes, are used as illustrative examples to demonstrate the robustness of the proposed model. Detailed description is given to show the coupling between the Monte Carlo model and the DRBEM formulation. Temperature transients, laser light energy distribution and coagulation patterns are reported for various LITT procedures.

2. Numerical method and algorithms

2.1. Dual reciprocity boundary element formulation

For simplicity, the two-dimensional problem is considered in this study. The well-known Pennes bioheat equation is used to model heat transfer in laser-irradiated tissues [27]:

$$\rho c_p \frac{\partial T}{\partial t} = \nabla \cdot (k \nabla T) + w_b \rho_b c_b (T_a - T) + q_m + q_l \tag{1}$$

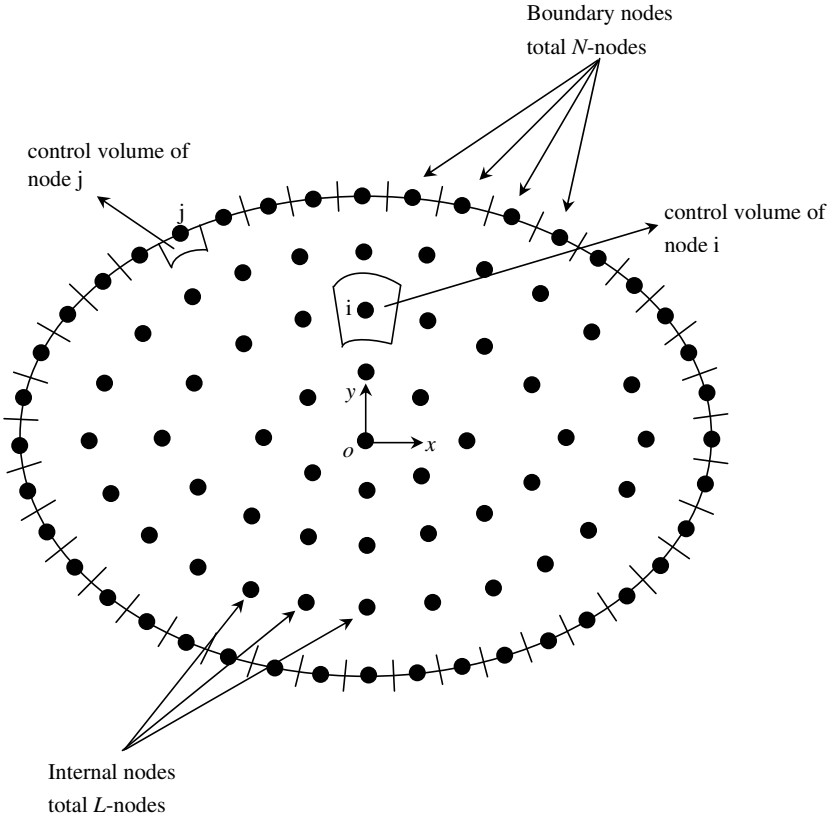

Fig. 3. DRBEM boundary and internal nodes and the coupling of the Monte Carlo results with the DRBEM.

For brevity, it is assumed that all the thermal and optical properties in this study are constant. Eq. (1) can be re-expressed in the following non-dimensional form:

$$\nabla^2 u = \frac{\partial u}{\partial \tau} + W_B \cdot u + D + Q_m + Q_l \tag{2}$$

with the dimensionless quantities defined as

$$u = \frac{T}{T_c}, \quad u_a = \frac{T_a}{T_c}, \quad \tau = \frac{\alpha t}{l_c^2}, \quad X = \frac{x}{l_c}, \quad Y = \frac{y}{l_c}$$
$$Q_m = -\frac{l_c^2 q_m}{kT_c}, \quad Q_l = -\frac{l_c^2 q_l}{kT_c}, \quad W_B = \frac{l_c^2 w_b \rho_b c_b}{k} \tag{3}$$
$$D = -\frac{l_c^2 w_b \rho_b c_b u_a}{k}$$

If all the right-hand terms of Eq. (1) are collectively represented by b, then Eq. (1) can be written in the following form:

$$\nabla^2 u = b \tag{4}$$

Clearly, b is a function of both time and space.

The solution of Eq. (4) can be expressed as the sum of the solution of Laplace's equation and a particular solution $\hat{u}$ for the Poisson equation $\nabla^2 \hat{u} = b$. Due to the difficulties of finding a solution $\hat{u}$, the dual reciprocity method uses a series of particular solution $\hat{u}_j$ instead of a single function $\hat{u}$. To this end, the source term b in Eq. (4) is firstly expanded in a series:

$$b \approx \sum_{j=1}^{N+L} f_j \alpha_j \tag{5}$$

where N is the number of BEM boundary nodes at which dual reciprocity points are collocated, L is the number of additional internal dual-reciprocity (DR) collocation points. The expansion functions f_j are specially chosen such that they satisfy the Poisson equation:

$$\nabla^2 \hat{u}_j = f_j \tag{6}$$

The expansion functions f_j can be of various types, but the radial basis functions (RBF) is proved to be the most successful by the extensive computational studies [24]. In this paper, the expansion functions f_j is chosen as $f_j = 1 + r_j$, where r_j is the radial distance from the DR collocation point j.

Substituting Eq. (5) into Eq. (4), one obtains

$$\nabla^2 u = \sum_{j=1}^{N+L} \alpha_j \nabla^2 \hat{u}_j \tag{7}$$

Multiplying both sides by the fundamental solution u^* of the Poisson equation, integrating over the whole computational domain, and using the Green's second identity on both sides result in the dual-reciprocity boundary integral equation:

$$c_i u_i + \int_\Gamma q^* u \, d\Gamma - \int_\Gamma u^* q \, d\Gamma = \sum_{j=1}^{N+L} \alpha_j \left(c_i \hat{u}_{ij} + \int_\Gamma q^* \hat{u}_j \, d\Gamma - \int_\Gamma u^* \hat{q}_j \, d\Gamma \right) \tag{8}$$

where c_i is a constant that only depends on the geometry at the node i; $q = \partial u/\partial n$, $q^* = \partial u^*/\partial n$, $\hat{q}_j = \partial \hat{u}_j/\partial n$ and n is the unit outward normal to the boundary surface of the solution domain. For two-dimensional problem considered here, u^*, q^*, $\hat{u}$, $\hat{q}$ can be derived as in [23,24].

By using the standard BEM discretization and collocating by taking the source point at the $i = 1, 2, \ldots, N+L$ boundary and interior nodes, Eq. (8) can be discretized as

$$c_i u_i + \sum_{k=1}^{N} H_{ik} u_k - \sum_{k=1}^{N} G_{ik} q_k = \sum_{j=1}^{N+L} \alpha_j \left(c_i \hat{u}_{ij} + \sum_{k=1}^{N} H_{ik} \hat{u}_{kj} - \sum_{k=1}^{N} G_{ik} \hat{q}_{kj} \right) \tag{9}$$

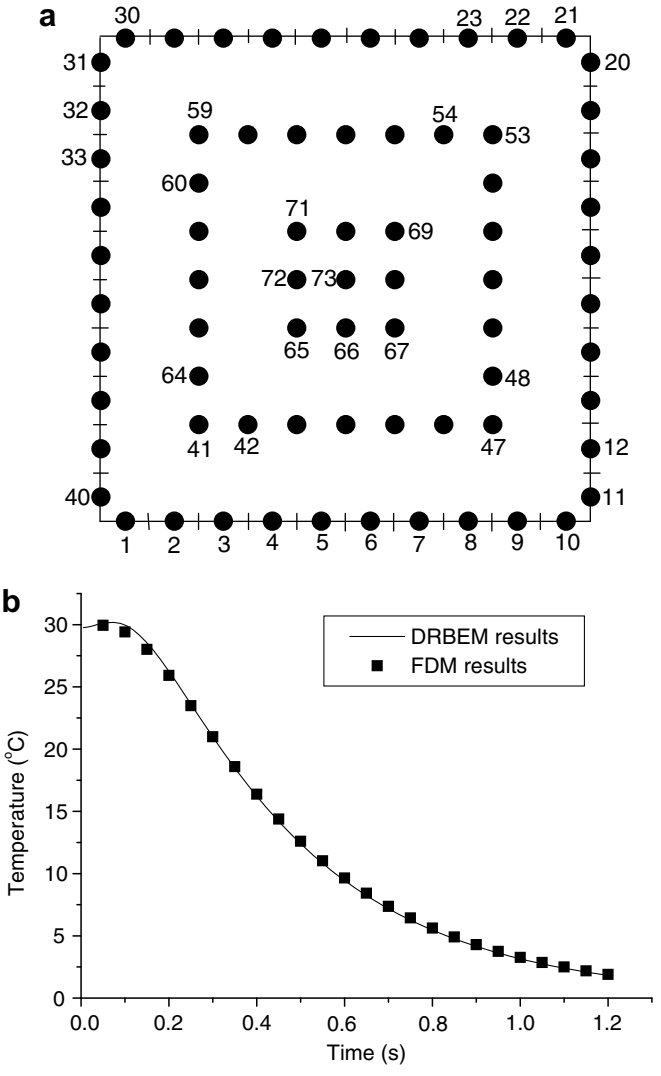

Fig. 4. Validation of the DRBEM computer code.

where $H_{ik} = \int_{\Gamma_k} q_i^* \, d\Gamma$, $G_{ik} = \int_{\Gamma_k} u_i^* \, d\Gamma$ for constant elements.

Eq. (9) can be expressed in a compact matrix form:

$$\mathbf{Hu} - \mathbf{Gq} = (\mathbf{H}\hat{\mathbf{u}} - \mathbf{G}\hat{\mathbf{q}})\boldsymbol{\alpha} \tag{10}$$

where $\mathbf{H}$ and $\mathbf{G}$ are the matrices of H_{ik} and G_{ik}, respectively (it should be noted that the c_i terms in Eq. (9) have been incorporated onto the diagonal of $\mathbf{H}$); The matrices $\mathbf{T}$, $\mathbf{q}$, $\widehat{\mathbf{T}}$ and $\hat{\mathbf{q}}$ correspond to vectors T_k, q_k, $\widehat{T}_{kj}$, and $\hat{q}_{kj}$, respectively; $\boldsymbol{\alpha}$ is the vector of the expansion coefficient α_j, which can be solved according to Eq. (5):

$$\alpha = \mathbf{F}^{-1}\mathbf{b} \tag{11}$$

where $\mathbf{F}$ is the matrix form of the function f; $\mathbf{b}$ is the vector of b_k.

According to Eq. (2), the vector $\mathbf{b}$ can be calculated as

$$\mathbf{b} = \dot{\mathbf{u}} + W_B\mathbf{u} + \mathbf{D} + \mathbf{Q}_m + \mathbf{Q}_l \tag{12}$$

where $\dot{\mathbf{u}}$ represents $\partial\mathbf{u}/\partial t$, and $\mathbf{D}$, $\mathbf{Q}_m$, $\mathbf{Q}_l$ are vectors arising from blood perfusion, metabolic heat generation and heat source due to laser light absorption.

A linear approximation is proposed for the variation of u, q within each time step, in the following form:

$$\dot{u} = \frac{1}{\Delta t}(u^{m+1} - u^m) \tag{13a}$$

$$u = (1-\theta_u)u^m + \theta_u u^{m+1} \tag{13b}$$

$$q = (1-\theta_q)q^m + \theta_q q^{m+1} \tag{13c}$$

where θ_u and θ_q are parameters which position the values of u and q between time level m and $m+1$. A series of tests carried out in [24] indicated that, in general, good accuracy can be obtained for the values θ_u and θ_q equal to 0.5 and 1.0, respectively.

Substituting Eqs. (11)–(13) into Eq. (10) yields

$$\left[\left(\frac{2}{\Delta\tau} + W_B\right)\mathbf{S} + \mathbf{H}\right]\mathbf{u}^{m+1} - 2\mathbf{G}\mathbf{q}^{m+1} = \left[\left(\frac{2}{\Delta\tau} - W_B\right)\mathbf{S} - \mathbf{H}\right]\mathbf{u}^m - 2\mathbf{S}(\mathbf{D} + \mathbf{Q}_m + \mathbf{Q}_l) \tag{14}$$

where $\mathbf{S} = -(\mathbf{H}\hat{\mathbf{u}} - \mathbf{G}\hat{\mathbf{q}})\mathbf{F}^{-1}$ and the values $\theta_u = 0.5$ and $\theta_q = 1.0$ have been used.

Applying the boundary conditions at time $(m+1)\Delta t$ and substituting the calculated results at the previous time $m\Delta t$, the unknown u and q at time $(m+1)\Delta t$ can be solved from the above equation.

In LITT clinics, the tumors are usually in contact with the healthy tissues or the ambient (for superficial tumors). In this study, the heat exchange between the tumors and the surrounding healthy tissues is considered as the boundary condition of the third kind at the tumor boundaries.

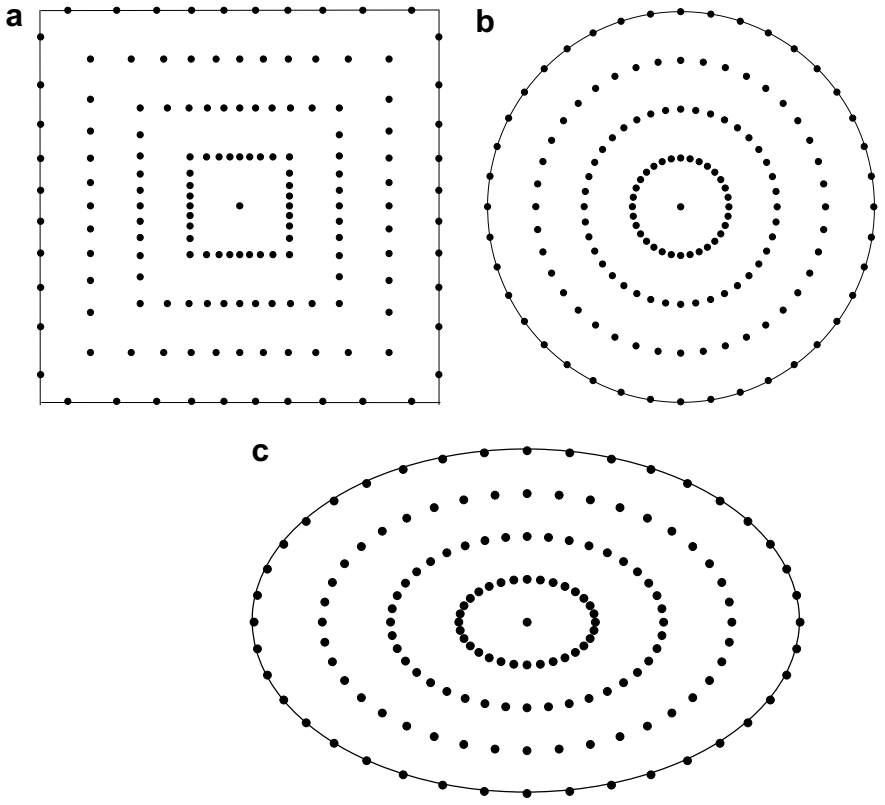

Fig. 5. Three tumor geometries and DRBEM discretizations considered in this study.

The implementation of the third kind boundary condition in a BEM model will not be mentioned here since it is available elsewhere (e.g. [24]).

In Eq. (14), the heat source terms due to blood perfusion and metabolism, $\mathbf{D}$ and $\mathbf{Q}_m$, are considered to be constant. However, the heat generation term arising from laser light absorption, $\mathbf{Q}_l$, is non-homogeneous and space-dependent, which can be obtained by the photon propagation simulation in the biological tissues.

2.2. Monte Carlo simulation of photon propagation in tissues

Light propagation in soft biological tissues is much more complicated than in industry solids. In biological tissues, light is both absorbed and scattered [28]. Scattering dominates in the red and near-infrared spectrum. This provides a therapeutic window for light penetration in tissue [2]. The most widely used theory describing the light propagation in biological tissues is the radiative transfer equation [2,3]:

$$\hat{s}\cdot\nabla L(\bar{r},\hat{s})+\mu_t L(\bar{r},\hat{s})=\frac{\mu_t}{4\pi}\int_{4\pi}p(\hat{s},\hat{s}')L(\bar{r},\hat{s}')\,\mathrm{d}\omega' \qquad (15)$$

The analytical solutions for the radiative transfer equation can be obtained only for very simple cases [3], e.g., one-dimensional geometry. Monte Carlo simulation [29] of photon propagation offers a flexible yet rigorous approach toward photon transport in turbid materials, like biological tissues, and it can easily deal with two- or three-dimensional problems with complex geometry. For these reasons, it has been widely used to simulate light transport in tissues for various applications (e.g., [30–32]). In this study, the Monte Carlo method will be employed to simulate the photon propagation in tissues with various geometries.

The Monte Carlo simulation is conducted in a three-dimensional (3-D) Cartesian coordinate system, as depicted in Fig. 1(a), where a square cylinder is used as the illustrative example and the symbol r_l denotes the radius of the laser beam spot (it is worth noting that r_l is not an input parameter for implanted fiber delivery cases). The origin of the coordinate system o is located at the center of the cylinder. Though the Monte Carlo simulation is carried out in a 3-D geometry, the DRBEM calculation described earlier is performed in a two-dimensional (2-D) geometry. Therefore, the Monte Carlo simulating results need to be

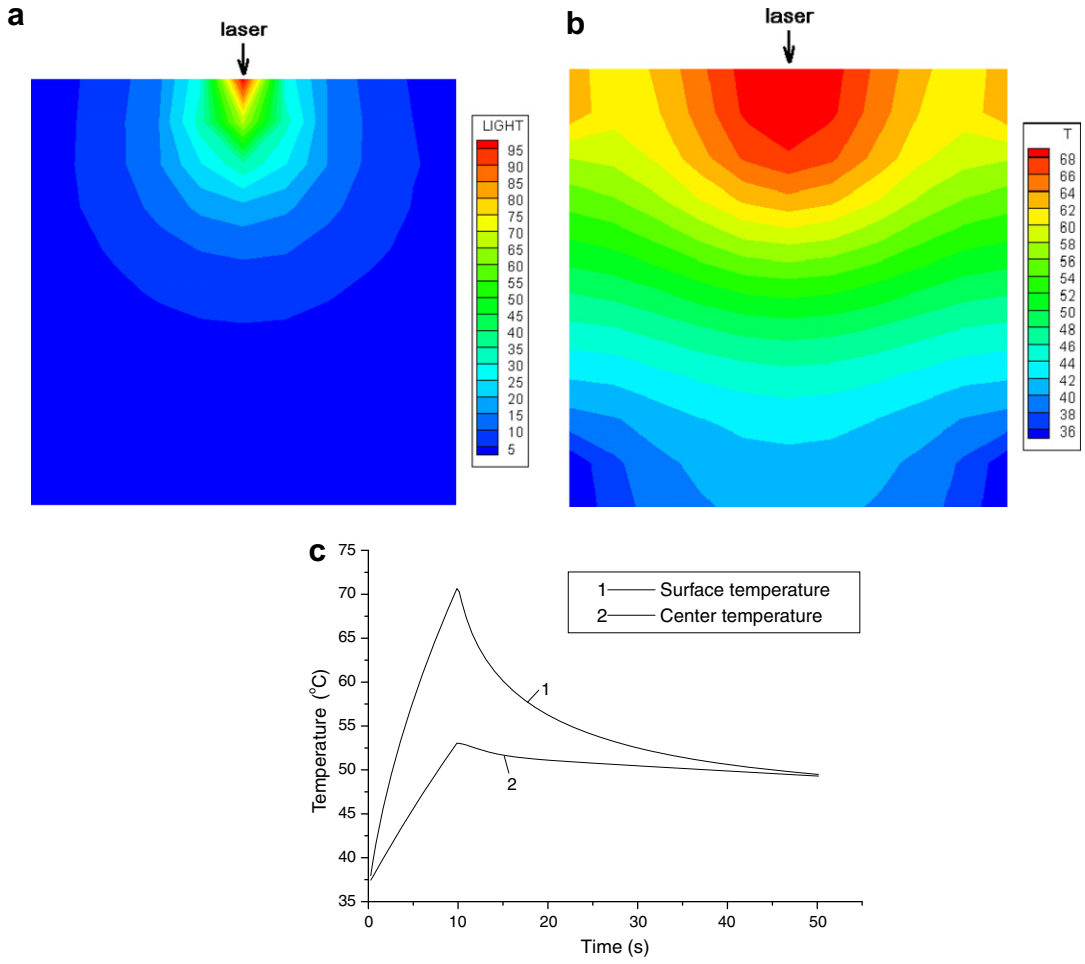

Fig. 6. Calculating results for square tumor when external laser beam irradiation is applied: (a) light distribution, (b) temperature distribution and (c) temporal evolution of temperature.

converted into 2-D results upon its completion. To this end, the dimension of the cylinder in y direction is intentionally chosen to be much longer than the x and z dimensions, as is noticed in Fig. 1(a). Through this method, the 2-D photon transport can be simulated in a 3-D geometry. Our calculations show that the simulating results are y-independent when the dimension of the cylinder in y direction is 10 times longer than the x and z dimensions. The 2-D Monte Carlo simulation devised in this study is suited for the description of the light propagation induced by an external rectangular laser beam or by an inserting cylindrical diffusively scattering fiber-tip. Fig. 1(b) shows the 2-D coordinate system, which is used to store the Monte Carlo simulating results at the mid-length plane in y direction. Such 2-D results are then incorporated into the DRBEM algorithm as the heat source due to laser light absorption. Other types of cylinders, e.g. circular and elliptic cylinders, are treated in a similar way.

For the external laser beam cases, a collimated flat-field beam with a radius r_l is considered. The launch position of photon is

$$x = r_1\sqrt{\xi_1} \quad \text{if } \xi_2 \geqslant 0.5 \tag{16a}$$

$$x = -r_1\sqrt{\xi_1} \quad \text{if } \xi_2 < 0.5 \tag{16b}$$

$$y = 2L_y\xi_3 - L_y \tag{16c}$$

$$z = 0.5L_z \tag{16d}$$

For the implanted fiber cases, the laser fiber tip is assumed to be diffusive, which can distribute the laser energy in all directions equally. The size of the fiber tip itself is considered to be negligible compared to that of the tissue. Therefore, the launching point of photon is at the same location where the fiber tip is. The launch direction of photon is determined by

$$\theta = \arccos(2\xi_1 - 1) \tag{17a}$$

$$\phi = 2\pi\xi_2 \tag{17b}$$

where θ is the deflection angle relative to z-axis and ϕ is the azimuthal angle. The direction cosine of the launching photon is

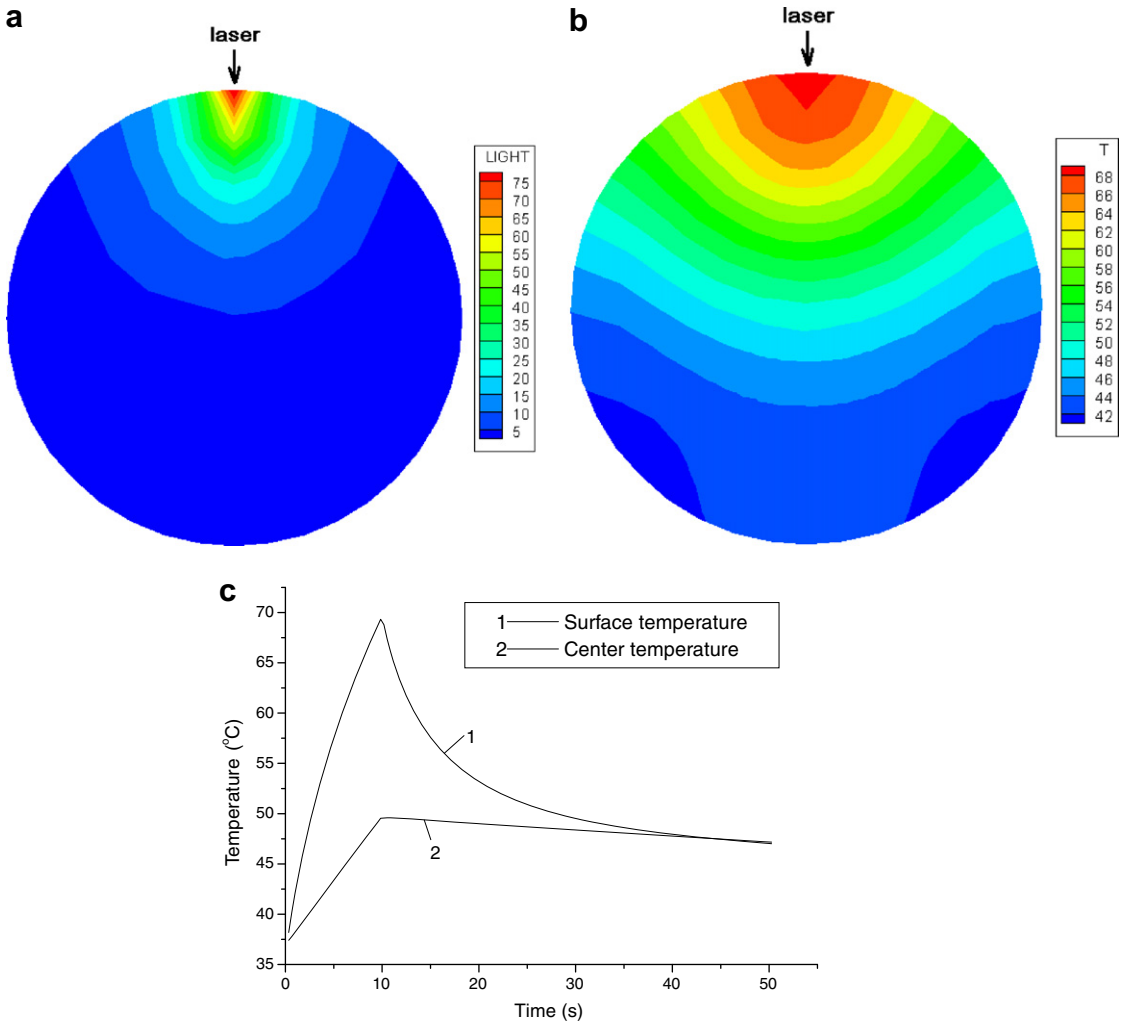

Fig. 7. Calculating results for circular tumor when external laser beam irradiation is applied: (a) light distribution, (b) temperature distribution and (c) temporal evolution of temperature.

$$\mu_x = \sin\theta\cos\phi \tag{18a}$$

$$\mu_y = \sin\theta\sin\phi \tag{18b}$$

$$\mu_z = \cos\theta \tag{18c}$$

Since the incident direction is in minus y direction and perpendicular to x–y plane, the initial direction cosine is [0,0,1]. If the refractive indices of the surrounding medium (healthy tissue, or air if the tumor is exposed to the ambient) and tissue are n_1 and n_2, respectively, then the specular reflectance, R_{sp}, is calculated by

$$R_{sp} = \frac{(n_1 - n_2)^2}{(n_1 + n_2)^2} \tag{19}$$

The photon weight, set initially to 1, is decremented to $1 - R_{sp}$.

The step size of the photon, s, between interaction sites is sampled according to the following equation:

$$s = -\ln(\xi)/\mu_t \tag{20}$$

Once the step size s is determined, the new position of the photon can be calculated by the current photon position and the current direction cosine values.

At the interaction point, a fraction of the photon weight, $(\mu_a/\mu_t)W$, will be deposited in the local grid element (x, y, z) due to absorption by tissue:

$$Q(x,y,z) \leftarrow Q(x,y,z) + (\mu_a/\mu_t)W \tag{21}$$

The new photon weight is $(\mu_s/\mu_t)W$.

In the Monte Carlo algorithm used in this study, only the photons falling into the grid elements at the mid-length plane in y direction need to be stored since only the absorption energies in this plane will be used as the input of the DRBEM computer code. Once the photon has been moved and its weight is decreased due to absorption, the photon is ready to be scattered. Algorithms for computing scattering

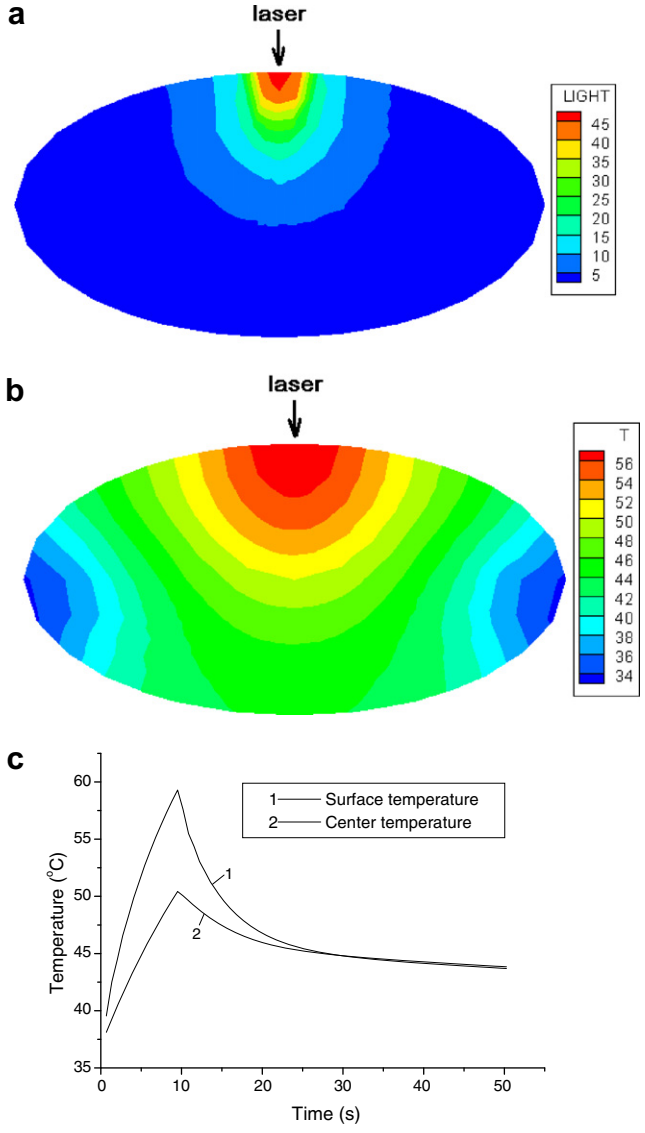

Fig. 8. Calculating results for elliptic tumor when external laser beam irradiation is applied: (a) light distribution, (b) temperature distribution and (c) temporal evolution of temperature.

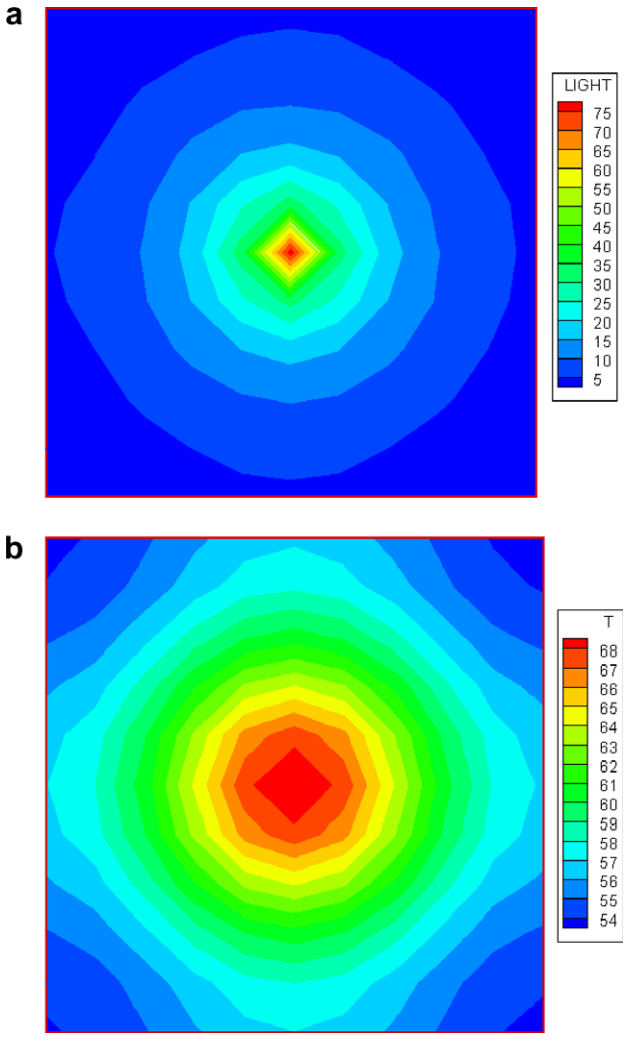

Fig. 9. Calculating results for square tumor when single laser fiber tip is applied at the tumor center: (a) light distribution and (b) temperature distribution.

angles and direction are described in detail elsewhere (e.g. [12,31]).

During a step of size s, the photon may cross the boundary of the tumor volumes. If this is the case, the photon may either escape as observed reflectance (or transmittance) or be internally reflected by the boundary. The probability of a photon being internally reflected depends on the angle of the incidence θ_i. The internal reflectance is calculated by Fresnel's law. Because the tumor geometries are considered to be arbitrary in this study, a general algorithm needs to be formulated to trace the photon traveling direction after reflection and transmittance at the boundary with complex shapes.

Fig. 2 shows the geometry when reflection and transmittance occur at a boundary, the two sides of which have different refractive indices. The unit vector $\vec{n}$ denotes the outward normal of the surface at the crossing point O. The direction cosine of $\vec{n}$ is expressed as (n_x, n_y, n_z). $-\vec{n}$ denotes the inward normal vector. The unit vectors AO, OB, and OF denote the incident direction, reflecting direction and refracting direction, respectively.

The angle of incidence θ_i, the angle between the incidence direction and the outward normal, is calculated by

$$\begin{aligned}\theta_i &= \arccos(-\vec{AO}\cdot\vec{n}) \\ &= \arccos[-(\mu_x n_x + \mu_y n_y + \mu_z n_z)]\end{aligned} \tag{22}$$

where " $\cdot$ " represents the scalar product of two vectors; (μ_x, μ_y, μ_z) denotes the current direction cosine of the photon.

The angle of transmittance θ_t can be calculated by Snell's law:

$$n_i \sin\theta_i = n_t \sin\theta_t \tag{23}$$

where n_i is the refractive index of the medium from which the photon is incident, n_t is the refractive index of the medium into which the photon is transmitted.

According to the parallelogram rule governing the addition of two vectors, shown in Fig. 2, the new direction after reflection, OB, can be calculated as

$$\vec{OB} = \vec{AC} = \vec{AO} + \vec{OC} = \vec{AO} + 2\cos\theta_i\,\vec{n} \tag{24}$$

As long as the equation describing the curved surface is known, the photon reflection and transmittance can be described for any tumor shapes using Eqs. (22)–(24).

A technique called Russian roulette [31] is used to terminate the photon propagation. If the photon has not survived a Russian roulette when its weight is below the threshold weight (e.g., 0.0001), the tracing of this photon is terminated, and a new photon is introduced.

The rate of heat generation due to laser light absorption at node i in the mid-length plane in y direction, $q_l[i]$, in the units of W/m^3, is calculated by the following relation:

$$q_l[i] = \frac{Q(x,z)P}{N_p V[i]} \tag{25}$$

where (x,z) is the location of the node i; N_p is the total photon number; $V[i]$ is the control volume of node i; P is the incident laser power.

Taking the elliptic cylinder as the illustrative example, Fig. 3 shows the distribution of DRBEM boundary and internal nodes and the coupling of the Monte Carlo simulation results with the DRBEM. A control volume is assigned to each DRBEM node (totally $N+L$ nodes). For clarity, we only show two control volumes for nodes i and j. To achieve higher accuracy, each DRBEM node should be located at the center of its control volume except the boundary nodes (e.g. j in Fig. 3). For the boundary nodes, the control volume should be chosen to be small enough such that the boundary node can be regarded as the representative point for that control volume. But the control volumes for boundary nodes cannot be too small since a very small control volume will carry little photon

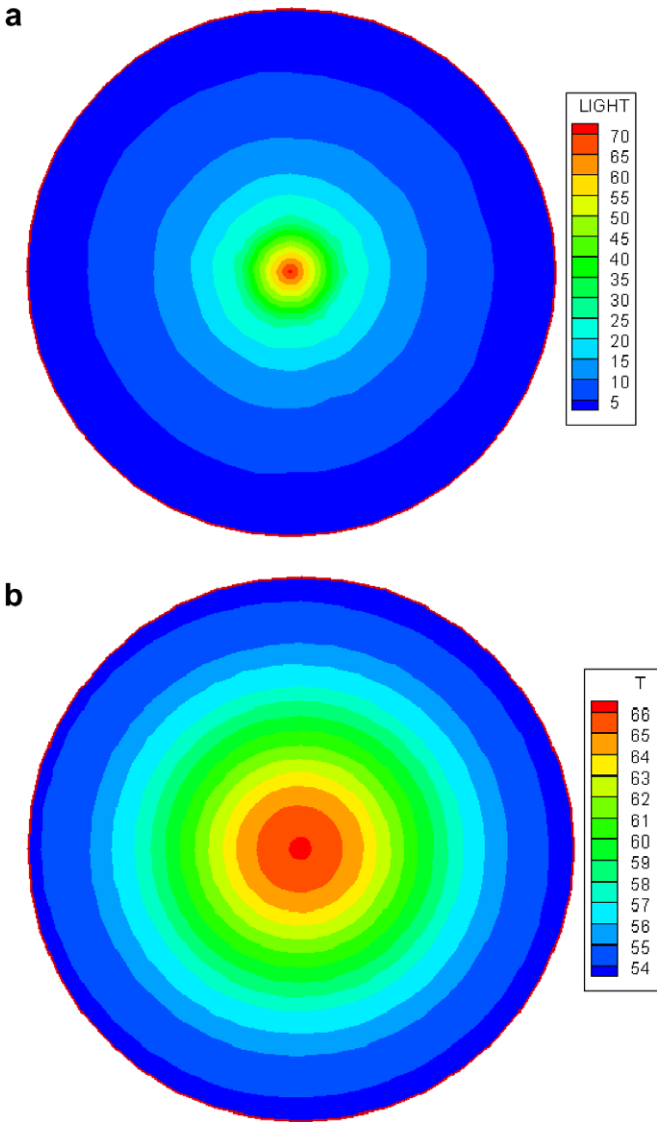

Fig. 10. Calculating results for circular tumor when single laser fiber tip is applied at the tumor center: (a) light distribution and (b) temperature distribution.

information. Therefore, there is a compromise in the choosing of the control volumes for boundary nodes. The choice of the control volume shape can be arbitrary. But it should be made certain that there is no overlap between any two control volumes. Otherwise, the same photon absorption event will be counted two times, which is physically unreasonable.

When a photon absorption event takes place in the process of Monte Carlo simulation process, some special computer codes need to be written to judge if the photon falls into the $N+L$ control volumes. If this is the case, Eq. (21) will be used to store the photon absorption energy.

3. Application examples

A FORTRAN computer code has been written based on the preceding description. The computer code must be validated before applied to calculate the light propagation and heat transfer in laser-irradiated biological tissues.

Consider the heat diffusion in a square plate initially at 30 °C. From time $t > 0$, the temperatures of all the boundaries are suddenly decreased to 0 °C. The side length of the square region is 3 m. The thermal diffusivity is 1.25 m^2/s. The time step interval is 0.05 s. There are 24 time steps in total. The boundary of the square region is discretized by 40 constant boundary elements and 33 internal nodes are used. The discretization is shown in Fig. 4(a). All the boundary and internal nodes are arranged in counterclockwise direction. Fig. 4(b) shows the temperature variation with time at the center point [i.e., node 73 in Fig. 4(a)]. As can be seen, the DRBEM results agree very well with those calculated by the finite difference method (FDM). The Monte Carlo computer code has been well validated in the authors' previous publications [12,33] and it will not be repeated here.

In the following, the numerical model developed above will be used to simulate the photothermal responses of biological tissues in laser-induced thermotherapy for several illustrative examples. The light and heat transport in three different tumor geometries, i.e., square, circle and ellipse, will be solved, as depicted in Fig. 5, to demonstrate the robustness of the proposed model. The distribution of the DRBEM boundary nodes and internal nodes are also shown in Fig. 5. Such a discretization is obtained by a refinement grid test on both boundary and internal nodes. It is worth pointing out that the symmetric distribution of

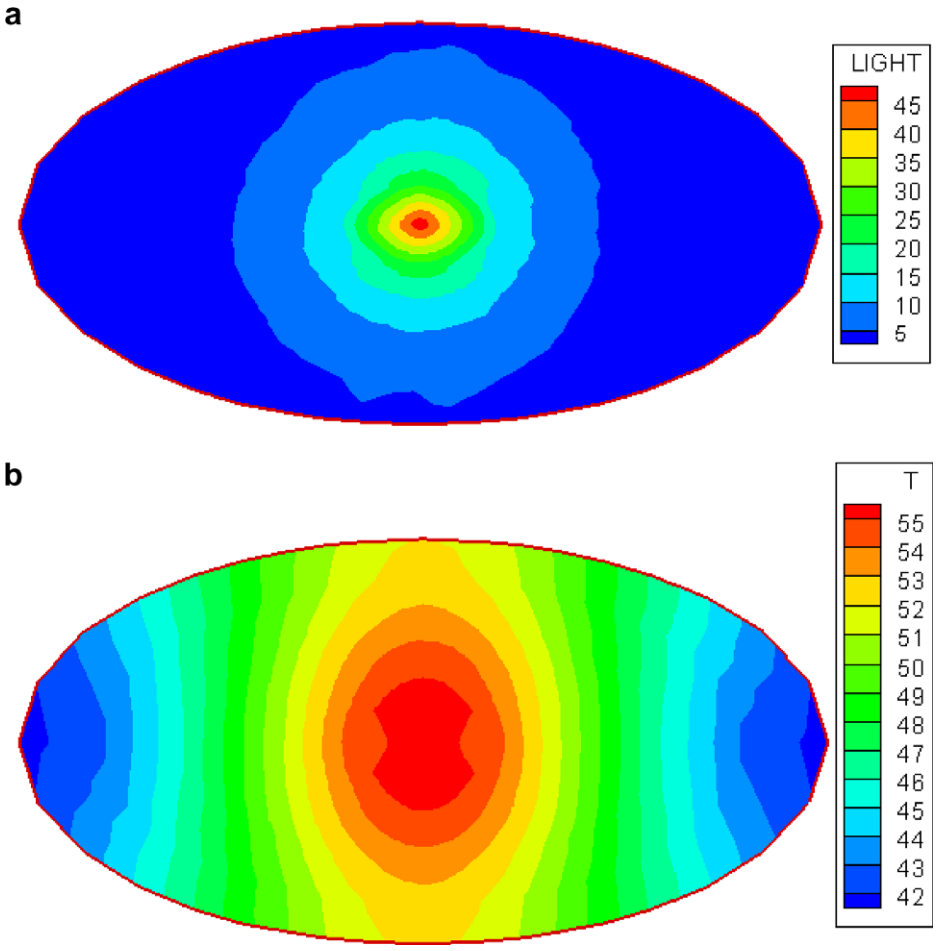

Fig. 11. Calculating results for elliptic tumor when single laser fiber tip is applied at the tumor center: (a) light distribution and (b) temperature distribution.

the internal nodes is just for illustrative simulation purpose. In fact, the choice of the internal nodes for a DRBEM model is not restricted to a symmetric configuration. One can select these nodes in any internal region of the domain based on requirement. The laser delivery modes can be either external laser beam irradiation or implanted fiber heating. The latter one corresponds to the interstitial laser thermotherapy (ILT). When the target volume is too large for treatment with a single fiber tip or when an irregular volume has to be treated, multiple fiber tips may be necessary for a single session treatment [4], which will also be examined in this section.

Unless otherwise specified, the following properties of a biological tissue are used in the numerical solutions: $\rho = 1000\ \text{kg/m}^3$, $k = 0.628\ \text{W/m K}$, $c_p = 4187\ \text{J/kg K}$, $w_b = 1.87 \times 10^{-3}\ \text{m}^3/\text{m}^3$ tissue s for the thermophysical properties [34]; $\mu_a = 1.0\ \text{cm}^{-1}$, $\mu_s = 100.0\ \text{cm}^{-1}$, anisotropy factor $g = 0.8$ and refractive index $n = 1.33$ for the optical properties, which are chosen based on the general data in the visible and near-infrared spectrum [35]. The thermal physical properties and temperature of arterial blood are [34]: $\rho_b = 1.06 \times 10^3\ \text{kg/m}^3$, $c_b = 3860\ \text{J/kg K}$, $T_a = 37\ ^\circ\text{C}$. The metabolic heat generation is $Q_m = 1.19 \times 10^3\ \text{W/m}^3$. The heat exchange occurring at the tumor boundaries are treated via a convective boundary condition in which an effective convection coefficient $h = 10\ \text{W/m}^2\ \text{K}$ and fluid temperature 20 °C are used.

Figs. 6–8 show the calculating results when the external laser beam heating mode is applied. For the sake of comparison, the three 2-D objects depicted in Fig. 5 have the same area though they take different shapes. Their sizes are chosen as follows. The half side length of the square tumor is $a = 2$ mm. The radius of the circle tumor is $1.13a$. The long and short radii of the ellipse tumor are $1.60a$ and $0.80a$, respectively. The laser power, heating duration, and spot radius are chosen as 10 W, 10 s, and 0.2 mm, respectively. Though a continuous wave laser is used for illustrative examples, the duration time of laser heating is a finite value. Therefore, the term "laser pulse" will still be used for the convenience of description. As is seen from the sub-figure (c) in Figs. 6–8, the temperatures at the laser spot center and tumor center firstly increase with time, reach a maximum value at the time when laser is turned off, and then fall down due to heat loss into the

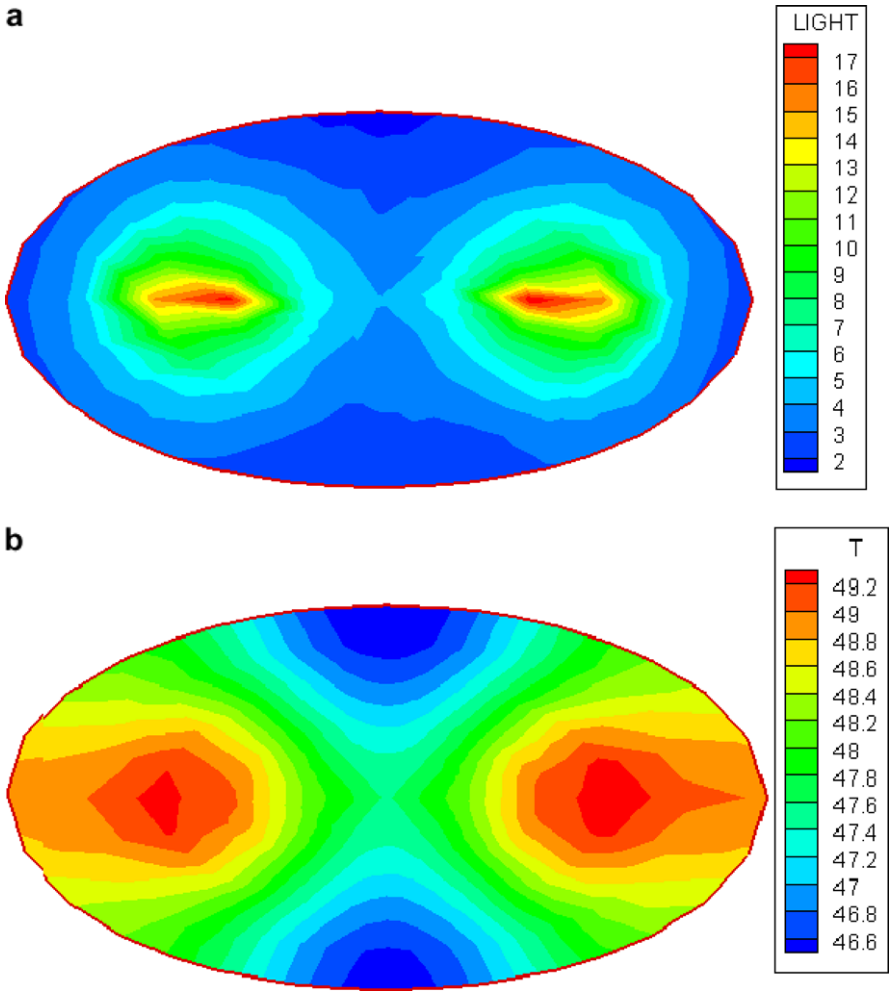

Fig. 12. Light energy and temperature distributions in the elliptic tumor when two laser fiber tips are applied at the same time.

surrounding tissues. Sub-figure (a) of Figs. 6–8 shows the volumetric heat generation (in W/cm^3) due to laser light absorption in tissue. It can be seen that under the same laser irradiation parameters and the same tumor bulk volume, the light energy converted to heat source for the square tumor shape is the highest among the three tumor shapes shown in Fig. 5. This is because that more photons will be transmitted out of the tumor volumes when the tumors take circular or elliptic shapes. Sub-figure (b) of Figs. 6–8 shows the temperature distribution at the time when the laser is turned off. As can be noticed, under the external heating mode, the temperatures inside the tumor volume are considerably non-uniform. The maximum temperature differences across the tumor bulk volume for square, circle and ellipse shapes are, respectively, 32, 26 and 22 °C. This leads to a failed surgery treatment since only part of the tumor cells can be killed through denaturization while the tumor cells in other parts are still alive and will continue to grow after this treatment session. To achieve complete coagulation of the tumor cells, one has to increase the laser irradiation power. This will inevitably cause severe traumatism and pain on the patients.

To realize effective tumor treatment, a complete photocoagulation is expected to be achieved and undesired damage to the surrounding healthy tissues should be avoided as possible as one can. Interstitial laser thermotherapy is a high efficient minimally invasive technique for the treatment of tumors. This surgery has been performed increasingly for local destruction of different tumors, which is performed by directly inserting the laser fiber tip into the center of the tumor bulk. However, the clinical application of ILT is still limited. One of the reasons is the limited capability of existing treatment planning models in accurately predicting the coagulation zone. The following simulations are intended to examine the applicability of the proposed DRBEM model in predicting the photothermal responses in interstitial thermotherapy procedure.

Figs. 9–11 show the simulation results when a single laser fiber tip is inserted into the center of the tumor bulk for square, circular and elliptic tumor geometries. The laser irradiation parameters and tumor sizes are the same as those in Figs. 6–8. As can be seen, when using the implanted fiber heating mode, the maximum temperature differences inside the whole tumor bulk volumes are 14, 12 and 13 °C for square, circular and elliptic tumors, respectively. This indicates that a uniform temperature elevation is achieved by the implanted laser fiber system.

Among the three types of tumors shown in Fig. 5, the elliptic tumor is irregular-type one since the two dimensions in x and z directions are quite different. For such irregular tumor volumes, multiple fiber system may be necessary for the best treatment effect. Fig. 12 shows the light energy and temperature distributions in the elliptic tumor when two laser fiber tips are inserted into the tumor volume at the same time. In this case, the power released by each fiber tip is 5 W and thus the total laser power is still 10 W. The locations of the two fiber tips are $x = 0.8a$, $z = 0$ and $x = -0.8a$, $z = 0$, respectively ($a = 2$ mm). It can be observed that the maximum temperature difference inside the elliptic tumor volume is reduced to 2.6 °C when two laser fiber applicators are applied at the same time. This clearly indicates that the optimal number of the laser fiber tips should be chosen based on the shape of the tumor.

For large size tumors, to implement successful therapeutic procedure, even two laser fiber tips may not be enough. Instead, multiple laser fiber tips may be necessary [4]. Fig. 13 shows the light energy and temperature distributions in the square tumor when four laser fiber tips are applied at the same time. The power for each of the fiber tip is 15 W. The half side length of the square tumor is $a = 4$ mm. The locations of the four fiber tips are $(x = 0.5a,\ z = 0.5a)$, $(x = -0.5a,\ z = 0.5a)$, $(x = -0.5a,\ z = -0.5a)$ and $(x = 0.5a,\ z = -0.5a)$. Other parameters are the same as those discussed above. It can be seen from Fig. 13 that for large size tumor, increasing the number of the fiber tips can achieve uniform temperature elevation.

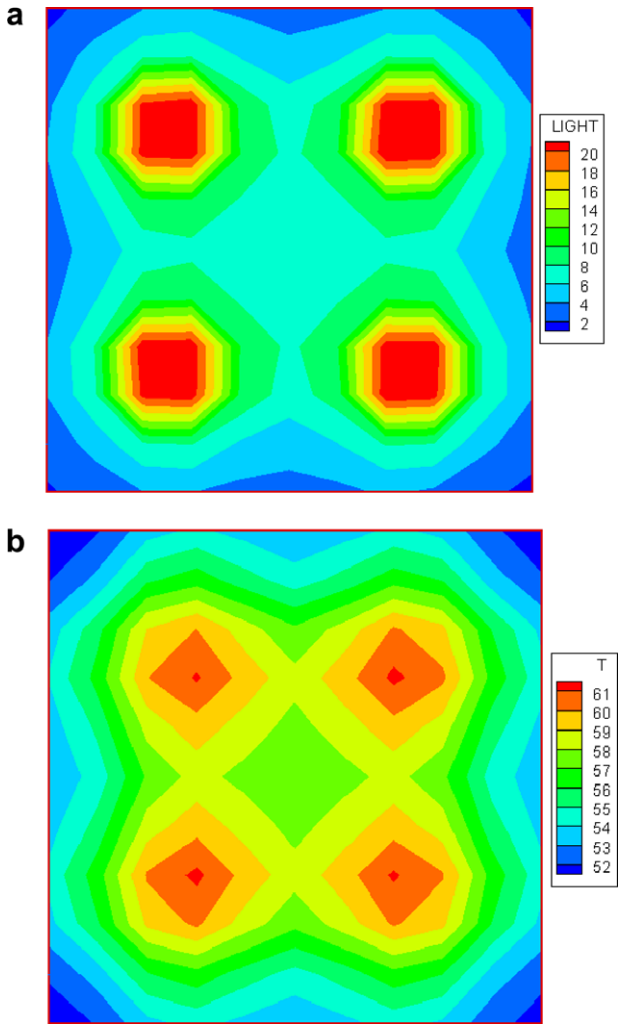

Fig. 13. Light energy and temperature distributions in the square tumor when four laser fiber tips are applied at the same time.

4. Conclusions

A two dimensional numerical model is developed to analyze the laser energy transport and heat transfer during laser-induced thermotherapy. The Monte Carlo approach is used simulate the photon propagation for both the external irradiation and implanted fiber cases. The dual reciprocity boundary element model is established to solve the bioheat equation to calculate the transient heat transfer in the laser-irradiated biological tissues. The coupling of the Monte Carlo approach and DRBEM model is described in detail. After the DRBEM model is validated against the finite difference method, the developed model is then used to simulate the photothermal response in LITT. Several typical tumor geometries are particularly considered to illustrate the applications of the present model. The calculating results show that the proposed DRBEM model can be used to deal with tumors with various geometrical shapes under different laser delivery modes with relative ease. The transient temperature variation, laser light energy distribution and coagulation patterns are clearly demonstrated for various cases, which are frequently encountered in clinics. Based on the requirements for inhibiting tumor growth and avoiding undesired damage to the surrounding normal tissues, an approach to optimize the treatment parameters can be obtained using the present DRBEM model.

References

[1] S.G. Bown, Phototherapy of tumors, World J. Surg. 7 (1983) 700–709.

[2] A.J. Welch, M.J.C. van Gemert, Optical-Thermal Response of Laser-Irradiated Tissue, Plenum Press, New York, 1995.

[3] M.H. Niemz, Laser-Tissue Interactions: Fundamentals and Applications, 2nd ed., Springer-Verlag, Berlin, 2002.

[4] K. Ivarsson, J. Olstrud, C. Sturesson, P.H. Moller, B.R. Persson, K.G. Tranberg, Feedback interstitial diode laser (805 nm) thermotherapy system: ex vivo evaluation and mathematical modeling with one and four-fibers, Lasers Surg. Med. 22 (1998) 86–96.

[5] A.M. Minhaj, F. Manns, P.J. Milne, D.B. Denham, N. Jr Salas, I. Nose, K. Damgaard-Iversen, J.-M. Parel, D.S. Robinson, Laser interstitial themotherapy (LITT) monitoring using high-resolution digital mammography: theory and experimental studies, Phys. Med. Biol. 47 (2002) 2987–2999.

[6] A.J. Welch, The thermal response of laser irradiated tissue, IEEE J. Quant. Electron 20 (12) (1984) 1471–1481.

[7] S.L. Jacques, S.A. Prahl, Modeling optical and thermal distributions in tissue during laser irradiation, Lasers Surg. Med. 6 (1987) 494–503.

[8] A. Sagi, A. Shitzer, A. Katzir, S. Akselrod, Heating of biological tissue by laser irradiation: theoretical model, Opt. Eng. 31 (7) (1992) 1417–1423.

[9] B. Anvari, S. Rastegar, M. Motamedi, Modeling of intraluminal heating of biological tissue: implications for treatment of benign prostatic hyperplasia, IEEE Trans. Biomed. Eng. 41 (1994) 854–864.

[10] L.B. Director, S.E. Frid, V.Y. Mendeleev, S.N. Scovorod'ko, Computer simulation of heat and mass transfer in tissue during high-intensity long-range laser irradiation, Ann. New York Acad. Sci. 858 (1998) 56–65.

[11] R.K. Shah, B. Nemati, L.V. Wang, S.M. Shapshay, Optical-thermal simulation of tonsillar tissue irradiation, Lasers Surg. Med. 28 (2002) 313–319.

[12] J. Zhou, J. Liu, Numerical study on 3-D light and heat transport in biological tissues embedded with large blood vessels during laser-induced thermotherapy, Numer. Heat Transfer Part A 45 (5) (2004) 415–449.

[13] S.C. Jiang, X.X. Zhang, Dynamic modeling of photothermal interactions for laser-induced interstitial thermotherapy: parameter sensitivity analysis, Lasers Med. Sci. 20 (2005) 122–131.

[14] H.J. Wang, W.Z. Dai, A. Bejan, Optimal temperature distribution in a 3D triple-layered skin structure embedded with artery and vein vasculature and induced by electromagnetic radiation, Int. J. Heat Mass Transfer 50 (2007) 1843–1854.

[15] S.B. Colak, M.B. van der Mark, G.W. 't Hooft, J.H. Hoogenraad, E.S. van der Linden, F.A. Kuijpers, Clinical optical tomography and NIR spectroscopy for breast cancer detection, IEEE J. Select. Top. Quantum Electron. 5 (4) (1999) 1143–1158.

[16] T.N. Glenn, S. Rastegar, S.L. Jacques, Finite element analysis of temperature controlled coagulation in laser irradiated tissue, IEEE Trans. Biomed. Eng. 43 (1) (1996) 79–87.

[17] S.H. Diaz, E.J. Lavernia, B.J.F. Wong, Modeling the thermal response of porcine cartilage during laser irradiation, IEEE J. Selected Top. Quant. Electron. 7 (6) (2001) 944–951.

[18] J.F. Verhey, Y. Mohammed, A. Ludwig, K. Giese, Implementation of a practical model for light and heat distribution using laser-induced thermotherapy near to a large vessel, Phys. Med. Biol. 48 (2003) 3595–3610.

[19] C.L. Chan, Boundary element method analysis for the bioheat transfer equation, ASME J. Biomech. Eng. 114 (1992) 358–365.

[20] C.A. Brebbia, J.C.F. Telles, L.C. Wrobel, Boundary Element Techniques, Springer, Berlin, 1984.

[21] L.C. Wrobel, The Boundary Element Method, Applications in Thermo-Fluids and Acoustics, vol. 1, Wiley, New York, 2002.

[22] A.J. Kassab, L.C. Wrobel, R.A. Bialecki, E.A. Divo, Boundary Element Method, in: W.J. Minkowycz, E.M. Sparrow, J.Y. Murthy (Eds.), Handbook of Numerical Heat Transfer, 2nd ed., Wiley, New York, 2006.

[23] D. Nardini, C.A. Brebbia, A new approach to free vibration analysis using boundary elements, in: C.A. Brebbia (Ed.), Boundary Elements in Engineering, Springer, Berlin, 1982.

[24] P.W. Partridge, C.A. Brebbia, L.C. Wrobel, The Dual Reciprocity Boundary Element Method, Elsevier Applied Science, London, 1992.

[25] J. Liu, L.X. Xu, Boundary information based diagnostics on the thermal states of biological bodies, Int. J. Heat Mass Transfer 43 (2000) 2827–2839.

[26] Z.-S. Deng, J. Liu, Modeling of multidimensional freezing problem during cryosurgery by the dual reciprocity boundary element method, Eng. Anal. Bound. Elem. 28 (2004) 97–108.

[27] H.H. Pennes, Analysis of tissue and arterial temperatures in the resting human forearm, J. Appl. Physiol. 1 (1948) 93–122.

[28] D.A. Benaron, W.-F. Cheong, D.K. Stevenson, Tissue optics, Science 276 (5321) (1997) 2002–2003.

[29] B.C. Wilson, A Monte Carlo model of the absorption and flux distributions of light in tissue, Med. Phys. 10 (6) (1983) 824–830.

[30] Y. Hasegawa, Y. Yamada, M. Tamura, Y. Nomura, Monte Carlo simulation of light transmission through living tissues, Appl. Opt. 30 (31) (1992) 4515–4520.

[31] L. Wang, S.L. Jacques, L. Zheng, MCML – Monte Carlo modeling of light transport in multi-layered tissues, Comput. Meth. Progr. Biomed. 47 (1995) 131–146.

[32] A.J. Welch, C.M. Gardner, Monte Carlo model for determination of the role of heat generation in laser-irradiated tissue, ASME J. Biomech. Eng. 119 (1997) 489–495.

[33] J. Zhou, J. Liu, A.B. Yu, Numerical study on the thawing process of biological tissue induced by laser irradiation, ASME J. Biomech. Eng. 127 (3) (2005) 416–431.

[34] Y. Yamada, T. Tien, M. Ohta, Theoretical analysis of temperature variation of biological tissues irradiated by light, in: L.S. Fletcher, T. Aihara (Eds.), Proceedings of the ASME/JSME Thermal Engineering Conference, vol. 4, Maui, Hawaii, 1995, pp. 575–581.

[35] W.F. Cheong, S.A. Prahl, A.J. Welch, A review of the optical properties of biological tissues, IEEE J. Quant. Electron. 26 (12) (1990) 2166–2185.